Proceedings of the ASME 2013 Fluids Engineering Division Summer Meeting
FEDSM2013
July 7-11, 2013, Incline Village, Nevada, USA

FEDSM2013-16567

EULERIAN-EULERIAN DESCRIPTION OF THE INTERACTION OF A SHOCK WITH PARTICLES THROUGH GODUNOV'S SCHEME

Quang Truong*
Department of Aerospace Engineering
and Engineering Mechanics
San Diego State University
San Diego, California 92182
qtruong@rohan.sdsu.edu

Babak Shotorban†
Department of Mechanical
and Aerospace Engineering
The University of Alabama in Huntsville
Huntsville, Alabama 35899
babak.shotorban@uah.edu

Gustaaf B. Jacobs‡
Department of Aerospace Engineering
and Engineering Mechanics
San Diego State University
San Diego, California 92182
gjacobs@mail.sdsu.edu

ABSTRACT

This paper is on an Eulerian-Eulerian (EE) approach that utilizes Godunov's scheme to deal with a running shock that interacts with a cloud of particles. The EE approach treats both carrier phase (fluid phase) and dispersed phase (particle phase) in the Eulerian frame. In this work, the fluid equations are the Euler equations for the compressible gas while the particle equations are based on a recently developed model to solve for the number density, velocity, temperature, particle sub-grid scale stresses, and particle sub-grid scale heat fluxes. The carrier and dispersed phases exchange momentum and heat, which are modeled through incorporating source terms in their equations. Carrier and dispersed phase equation form a hyperbolic set of differential equations, which are numerically solved with Godunov's scheme. The numerical solutions are obtained in this work for a two-dimensional normal running shock interacting with a rectangular cloud of particles. The results generated by the EE approach were compared against the results that were generated by a well-stablished Eulerian-Lagragian (EL) approach that treats the carrier phase in an Eulerian frame, while does the dispersed phase in a Lagrangian framework where individuals particles are traced and solved. For the considered configuration, the EE approach reproduced the EL results with a very good accuracy.

*Graduate Student.
†Assistant Professor; Member of ASME; All correspondence should be addressed to this author.
‡Associate Professor; Member of ASME

NOMENCLATURE

m_p	Mass of a particle
Pr	Prandtl number
t	Time variable
$\mathbf{Q}$	Solution
$\mathbf{F}$	Flux in x-direction
$\mathbf{G}$	Flux in y-direction
$\mathbf{S}$	Source term
u, u_i, $\mathbf{u}$	Fluid velocity
p	Pressure
T	Temperature of fluid
E	Total Energy
x, x_i, $\mathbf{x}$	Position
v, v_i, $\mathbf{v}$	Particle velocity
q_{ij}	Particle sub-grid scale heat

Greek symbols

ρ_f^*	Reference density
β	Ratio of particle heat capacity to fluid heat capacity at constant pressure
γ	Ratio of gas heat capacities
θ	Particle temperature
λ	Eigenvalues of Jacobian matrix
μ	Fluid viscosity
ρ	Fluid density
τ_p	Particle relaxation time constant
τ_T	Particle thermal relaxation time constant

ϕ	Particle number density
$\widetilde{v_i v_j}$	Second moment of particle velocity
$\widetilde{\theta v_i}$	Second moment of particle temperature and velocity
σ_{ij}	Particle sub-grid scale stress

Superscripts

T	Matrix Transpose

Subcripts

p	Particle, or Particle variable in the Lagrangian frame
f	Fluid
x	x-component
y	y-component

INTRODUCTION

A particle-laden flow belongs to a class of two-phase flows, in which a fluid (carrier phase) carries a very large number of small solid or liquid particles (dispersed phase). Such a flow can be seen in many areas including aerosol transport [1], fluidization [2] and volcanic eruption [3].

The carrier phase is typically modeled by conservation laws of mass, momentum and energy in the Eulerian frame while particles are individually traced in the Lagrangian frame. This is the Eulerian-Lagrangian approach (EL) to deal with the particle-laden flows. In the EL model, each particle is traced through solving for its position and velocities. In case the interaction of particles with the fluid is non isothermal, the temperature of the particle is also solved. The influence of particles on the carrier phase is taken into account by interpolating their properties from their locations to neighboring computational cells, and coupling to the carrier phase equations through source terms. This coupling Particle-Source-In-Cell (PSIC) model was pioneered by Crowe et *al* [4]. Jacobs et *al*. [5, 6] present a third and fifth order (WENO-Z) accurate scheme to solve the PSIC EL model. Jacobs and Don [5] solved a one and two dimensional particle-laden flow problem, where a shock wave encounters a cloud of particles. The benefit of the EL model is reduced computational time by grouping small particles into a larger particle [6–8]. Moreover, the EL model shows higher accuracy because it calculates the particles' properties without averaging. The main drawback of the EL is when one requires to get insight into the particle concentration (or equivalently the particle number density) as a very large number of particles need to be traced to have enough samples for calculating this quantity through averaging.

In the Eulerian-Eulerian (EE) approach, particles are collectively modeled as continuum in the Eulerian frame similar to the carrier phase. The main advantage of the EE model is that it readily provides the information about the number density of particles as it is one of the dependent variables for which the partial differential equations are solved for. Other statistical information about the other properties of the particles such as their averaged velocity and temperature can be calculated as they are also dependent variables in the set of PDEs. A complete review on two-fluid models is beyond the scope of this work; however, interested readers are referred to Refs. 9–14.

The current work is concerned with an EE approach which is applied to study a running shock that interacts with a cloud of particles in a two-dimensional configuration. The approach is originated in an EE model [15] developed for the numerical simulation of isothermal particle-laden flows. Recently, Ortiz [16] extended this model to include non-isothermal cases. Furthermore, he utilized the model to study the interaction of a compressible flow with a cloud of particles in a one-dimensional configuration. Ortiz [16] used a first order Godunov scheme with Roe's averaging in his EE study. He tested the EE results against an EL model based on the WENO-Z PSIC scheme [5, 6] in a one-dimensional flow. A good agreement between EE and EL results was observed. For the supersonic case, the discrepancies between two models are higher than the subsonic case.

GOVERNING EQUATIONS

In this section, the equations that are solved in the considered two-phase particle-laden flows are presented.

Carrier Phase Equations

We assume that the carrier phase is governed by the Euler equations, a set of equations for inviscid flows representing conservation of mass, momentum, and energy. The Euler equations for the carrier phase are coupled to dispersed phase through source terms. We consider convection dominated flows, for which the viscous forces are relatively small. Thus, the viscous Navier-Stokes equations reduce to the following inviscid Euler equations expressed in dimensionless form:

$$\frac{\partial \mathbf{Q}_f}{\partial t} + \frac{\partial \mathbf{F}_f}{\partial x} + \frac{\partial \mathbf{G}_f}{\partial y} = \mathbf{S}_f \tag{1}$$

where

$$\mathbf{Q}_f = \left[\rho, \quad \rho u_1, \quad \rho u_2, \quad E\right]^T, \tag{2}$$

$$\mathbf{F}_f = \left[\rho u_1, \quad \rho {u_1}^2 + p, \quad \rho u_1 u_2, \quad (E+p)u_1\right]^T, \tag{3}$$

$$\mathbf{G}_f = \left[\rho u_2, \quad \rho u_1 u_2, \quad \rho {u_2}^2 + p, \quad (E+p)u_2\right]^T, \tag{4}$$

$$\mathbf{S}_f = \begin{bmatrix} 0 \\ \frac{m_p\phi}{\tau_p}(v_1 - u_1) \\ \frac{m_p\phi}{\tau_p}(v_2 - u_2) \\ \frac{\beta m_p \phi(\theta - T)}{(\gamma-1)\tau_T} + \frac{m_p\phi\left(\sigma_{11}+v_1^2-u_1v_1+\sigma_{22}+v_2^2-u_2v_2\right)}{\tau_p} \end{bmatrix}, \quad (5)$$

$$E = \frac{p}{\gamma-1} + \frac{1}{2}\rho\left({u_1}^2 + {u_2}^2\right). \quad (6)$$

The fluid is assumed an ideal gas therefore:

$$p = \frac{\rho T}{\gamma}. \quad (7)$$

Particle Phase Equations

The Lagrangian equations for the displacement, velocity, and temperature of a particle, respectively, are:

$$\frac{d\mathbf{x}_p}{dt} = \mathbf{v}_p, \quad (8)$$

$$\frac{d\mathbf{v}_p}{dt} = \frac{1}{\tau_p}(\mathbf{u}_f - \mathbf{v}_p), \quad (9)$$

$$\frac{d\theta_p}{dt} = \frac{1}{\tau_T}(T_f - \theta_p). \quad (10)$$

Eq. (9) is based on the assumption that the particle is only under the influence of the Stokes drag force. Eq. (10) is based on the assumption the the temperature within the solid particle is uniform and heat transfer to the particle from the surrounding gas-phase is modeled through Newton's heat convection law.

In order to develop the particle Eulerian equations, a Liouville equation, which governs the fine-grain density function in the phase (state) space, is first formulated, using the Lagrangian equations. Then, using a spatial filtering operator, the Liouville equation is filtered and a transport equation is obtained for the filtered density function. Averaging and obtaining the first and second moments of this equation with respect to velocities and temperature, results in a coupled system of Eulerian equations for the particle number density, velocity and temperature and their second moments in the physical space, i.e., ϕ, v_i, θ, $\widetilde{v_i v_j}$, and $\widetilde{\theta v_i}$, which are the number density, Eulerian velocity at i direction, Eulerian temperature of the particles, and second moments, respectively. The details of the particle-phase Eulerian formulation can be found in Ref. 15 for the isothermal case (without temperature) and in Ref. 16, for the non-isothermal case

Defining the sub-grid-scale particle stress σ_{ij}, and the sub-grid-scale particle heat flux q_i by:

$$\sigma_{ij} = \widetilde{v_i v_j} - v_i v_j, \quad (11)$$

$$q_i = \widetilde{\theta v_i} - \theta v_i, \quad (12)$$

the particle-phase Eulerian equations can be shown in the following conservative form:

$$\frac{\partial \mathbf{Q}_p}{\partial t} + \frac{\partial \mathbf{F}_p}{\partial x} + \frac{\partial \mathbf{G}_p}{\partial y} = \mathbf{S}_p, \quad (13)$$

where

$$\mathbf{Q}_p = \begin{bmatrix} \phi \\ \phi v_1 \\ \phi v_2 \\ \phi\theta \\ \phi(\sigma_{11}+v_1^2) \\ \phi(\sigma_{12}+v_1v_2) \\ \phi(\sigma_{22}+v_2^2) \\ \phi(q_1+\theta v_1) \\ \phi(q_2+\theta v_2) \end{bmatrix} = \begin{bmatrix} Q_1 \\ Q_2 \\ Q_3 \\ Q_4 \\ Q_5 \\ Q_6 \\ Q_7 \\ Q_8 \\ Q_9 \end{bmatrix}, \quad (14)$$

$$\mathbf{F}_p = \begin{bmatrix} Q_2 \\ Q_5 \\ Q_6 \\ Q_8 \\ -(2Q_2^3)/Q_1^2 - (3Q_2Q_5)/Q_1 \\ (2Q_2Q_6+Q_3Q_5)/Q_1 - (2Q_2^2Q_3)/Q_1^2 \\ (Q_2Q_7+2Q_3Q_6)/Q_1 - (2Q_2Q_3^2)/Q_1^2 \\ (Q_4Q_5+2Q_2Q_8)/Q_1 - (2Q_2^2Q_4)/Q_1^2 \\ (Q_4Q_6+Q_2Q_9+Q_3Q_8)/Q_1 - (2Q_2Q_3Q_4)/Q_1^2 \end{bmatrix}, \quad (15)$$

$$\mathbf{G}_p = \begin{bmatrix} Q_3 \\ Q_6 \\ Q_7 \\ Q_9 \\ (2Q_2Q_6+Q_3Q_5)/Q_1 - (2Q_2^2Q_3)/Q_1^2 \\ (Q_2Q_7+2Q_3Q_6)/Q_1 - (2Q_2Q_3^2)/Q_1^2 \\ -(2Q_3^3)/Q_1^3 - (3Q_3Q_7)/Q_1^2 \\ (Q_4Q_6+Q_2Q_9+Q_3Q_8)/Q_1 - (2Q_2Q_3Q_4)/Q_1^2 \\ (Q_4Q_7+2Q_3Q_9)/Q_1 - (2Q_3^2Q_4)/Q_1^2 \end{bmatrix}, \quad (16)$$

$$
\mathbf{S}_p = \begin{bmatrix}
0 \\
\frac{\phi}{\tau_p}(u_1 - v_1) \\
\frac{\phi}{\tau_p}(u_2 - v_2) \\
\frac{\phi}{\tau_T}(T - \theta) \\
-2\frac{\phi}{\tau_p}({v_1}^2 - u_1 v_1 + \sigma_{11}) \\
-\frac{\phi}{\tau_p}(2\sigma_{12} - u_1 v_2 - u_2 v_1 + 2 v_1 v_2) \\
-2\frac{\phi}{\tau_p}({v_2}^2 - u_2 v_2 + \sigma_{22}) \\
-\frac{\phi}{\tau_T}(q_1 - T v_1 + \theta v_1 + \theta v_2) - \frac{\phi}{\tau_p}(q_1 - \theta u_1 + \theta v_1 + \theta v_2) \\
-\frac{\phi}{\tau_T}(q_2 - T v_2 + \theta v_1 + \theta v_2) - \frac{\phi}{\tau_p}(q_2 - \theta u_2 + \theta v_1 + \theta v_2)
\end{bmatrix}. \quad (17)
$$

NUMERICAL METHODS

In this work, the flux terms, i.e., $\mathbf{F}_f$ and $\mathbf{G}_f$ in equation (1) and $\mathbf{F}_p$ and $\mathbf{G}_p$ in eq. (13), will be handled with Godunov's method [18]. It is borne in mind that these equations are hyperbolic partial differential equations in a conservative form for which Godunov's method is an efficient method to employ.

Let us assume that the domain is rectangular and discretized with a uniform Cartesian grid, defined by $x_i = i\Delta x$ and $y_j = j\Delta y$, where $i, j = 0, 1, 2, \ldots, N$ (number of grid points in each direction). The value $Q^n_{(i,j)}$ represents average of a cell with boundaries at $x_{i-1/2}$, $x_{i+1/2}$, $y_{i-1/2}$, and $y_{i+1/2}$. For a two dimensional hyperbolic equation in the general form of

$$
\frac{\partial \mathbf{Q}}{\partial t} + \frac{\partial \mathbf{F}}{\partial x} + \frac{\partial \mathbf{G}}{\partial y} = \mathbf{S}. \quad (18)
$$

fluxes $\mathbf{F}$ and $\mathbf{G}$ in Godunov's scheme are obtained by flux-vector splitting [18]

$$
\mathbf{F}_{i-1/2,j} = f(\mathbf{Q}^{\downarrow}_{i-1/2,j}) = \mathbf{A}^{+}_{i-1,j}\mathbf{Q}_{i-1,j} + \mathbf{A}^{-}_{i,j}\mathbf{Q}_{i,j}, \quad (19)
$$

$$
\mathbf{G}_{i,j-1/2} = f(\mathbf{Q}^{\downarrow}_{i,j-1/2}) = \mathbf{B}^{+}_{i,j-1}\mathbf{Q}_{i,j-1} + \mathbf{B}^{-}_{i,j}\mathbf{Q}_{i,j}, \quad (20)
$$

where $\mathbf{A} = \partial\mathbf{F}/\partial\mathbf{Q}$ and $\mathbf{B} = \partial\mathbf{G}/\partial\mathbf{Q}$ are the Jacobian matrices. In these equations, superscripts $+$ and $-$ indicate the respective decomposed positive- and negative-definite matrices.

In eq. (18), the source term $\mathbf{S}$ is decomposed into x and y components:

$$
\mathbf{S} = \mathbf{S}_x + \mathbf{S}_y, \quad (21)
$$

The x-direction component of the source term, $\mathbf{S}_x$, is similar to the one dimensional source term, with the y-direction components being 0. Here, $\mathbf{S}_y$ is determined from equation (21). Similarly, the particle source term from equation (17) are split.

In the x-direction, we solve one dimensional problem with j fixed, updating $\mathbf{Q}^n_{i,j}$ to $\mathbf{Q}^*_{i,j}$:

$$
\mathbf{Q}^*_{i,j} = \mathbf{Q}^n_{i,j} - \frac{\Delta t}{\Delta x}(\mathbf{F}^n_{i+1/2,j} - \mathbf{F}^n_{i-1/2,j}) + \Delta t \mathbf{S}_{x(i,j)}, \quad (22)
$$

while in the y-direction, we use $\mathbf{Q}^*_{i,j}$ for solving one dimensional problem with i fixed, to obtain $\mathbf{Q}^{n+1}_{i,j}$:

$$
\mathbf{Q}^{n+1}_{i,j} = \mathbf{Q}^*_{i,j} - \frac{\Delta t}{\Delta y}(\mathbf{G}^n_{i,j+1/2} - \mathbf{G}^n_{i,j-1/2}) + \Delta t \mathbf{S}_{y(i,j)}, \quad (23)
$$

This scheme will introduce a splitting error; however, it is often no more critical than the errors by the numerical methods in each sweep [18]. Also, dimensional splitting is only at best second order accurate; if a very high order method is applied, it is crucial to overcome this dimensional splitting error.

The CFL condition is a necessary condition for stability and convergence of a finite volume method for a PDE [18]. For the two dimensional case, we have two stability conditions, in the x-direction and in the y-direction. To ensure stability in both directions, the CFL condition becomes

$$
\Delta t = \mathrm{CFL}\frac{\min(\Delta x, \Delta y)}{\max(|\lambda^F_p|, |\lambda^G_p|)}. \quad (24)
$$

RESULTS AND DISCUSSIONS

We initialize a moving shock with M_S = 3.0 at x_S = 0.175 in a rectangular domain of $[0,1] \times [-0.2, 0.2]$. The fluid pre-shock properties are $\rho = 1$, $u = 0$, $v = 0$, and $p = 1$. In our simulations 40,000 particles with density ρ_p = 1000, diameter d = 5.7693×10^{-3}, and zero velocity, are uniformly distributed inside a rectangular cloud located at $[0.175, 0.352] \times [-0.05, 0.05]$. The particle relaxation and thermal time constants are set to τ_p = τ_T = 1. Tables 1 through 3 summarize the initial conditions of the problem. The computational mesh used is 600×200. For the same configuration, EL simulations are also conducted, employing the method of Ref. 5, to validate the EE results.

Fig. 1 shows a grid resolution study for the EE results based on the variation of the fluid density along the line of symmetry. It is seen that the improvement of the results of the resolutions 600×200 and 300×200 are fairly close. At $y = 0$ and $x = 0.45$, the local error between grid size of 400×200 and 600×200 are 2.343%. The use of grid size of 600×200 is justified.

In Figure 2, the particle number density ϕ is plotted versus x at time $t = 0.1$. At this early state, the leading edge of the cloud is pushed downstream by the moving shock. The cloud of particles experiences the moving shock first at its leading edge, causing a raise in particle velocity v_1 at that area. The bow shock created by interaction between fluid and the particle cloud increases v_1 even higher at the two corners of the leading edge. Behind the cloud, the flow separates; the trailing edge of the cloud does not interact with the fluid, causing a difference in velocity v_1 between the two end corners and the trailing edge of the cloud. Therefore, the leading edge of the cloud moves to the right and spreads outward to both sides in the y-direction while only the corners of the trailing edge move inward and downstream. The deformation of the particle cloud can be explained through the examination of the particle velocity v_1, which is plotted in Figure 3. It is seen that v_1 has higher values where the cloud contacts with the fluid. The higher v_1 is, the more likely the particles tend to travel away, and vice versa.

In Figure 4, the contour plots of the fluid density are seen. At time $t = 0.1$, the moving shock has run through the rectangular cloud. The area where the normal shock and the cloud come into contact creates a rise in fluid density, causing a bow shock at the front end, curving symmetrically in the y-direction. At the rear end of the moving shock when the curved shocks have passed the symmetry line, a Mach reflection is created. There is also a circulation created behind the particle cloud, similar to a flow over a blunt body. Even though at the same number of grid points as EE models, the WENO-5 EL shows more detail of the fluid, especially in the circulation and reflection area behind the cloud. The first order EE presents a very smooth plot of the fluid density.

In Figure 5, the fluid variables ρ, u_1, p, T, and Mach number, M are plotted against x on the symmetry line y = 0 at $t = 0.1$. In order to gain an insight into the accuracy of the EL simulation, the third order (WENO-3) plotted along with WENO-5. It is seen that their results are slightly different. Since the y-direction velocity v is relatively small, the local Mach number is plotted instead. At the front end of the cloud cloud, a sudden rise is seen for the fluid density, pressure, and temperature whereas a drop is seen for velocity and Mach number. The discrepancies between EE and EL are higher at the tailing edge the cloud. It is also seen that the shockwave in WENO-Z EL models travels slightly further distance when compared to that in the EE model. Moreover, based on fluid density and temperature plots, the differences between the EE and WENO-3 models are smaller compared to the differences between the EE and WENO-5 models. That means those discrepancies between three models behind the cloud might be caused by the difference in order of accuracy.

The particle velocity component in the x direction v_1 and temperature θ for both EE and EL models are displayed in Fig. 6. For both of these quantities, the models agree fairly well with each other. At this early time of t = 0.1, the trailing edge of the cloud contacts with the moving shock from left to right, causing higher velocity and temperature on the left, and lowering values as we move downstream.

SUMMARY AND CONCLUSIONS

A recently developed Eulerian-Eulerian (EE) model was utilized for the numerical study of a running shock interacting with a cloud of particles in a two-dimensional configuration. The EE model couples the inviscid Euler equations to a new set of Eulerian equations for the dispersed phase. The transport equations are for the particle number density, velocity, temperature, subgrid-scale stress, and sub-scales heat flux. The current study was the extension of the previous study from a one-dimensional configuration to a two-dimensional configuration.

The EE model is in the form of two sets of hyperbolic differential equations for the carrier and dispersed phase. The phases are coupled through source terms which account for the momentum and heat exchanges. The equations were discretized based on a finite volume method, and Godunov's scheme. The results obtained by the EE model was compared against the results obtained by a recently developed Eulerian-Langrangian (EL) model in which particles are dealt with in the Lagrangian frame, and good agreement were observed between them.

ACKNOWLEDGMENT

The support for this work was provided by the National Science Foundation under grant numbers DMS-1115631 and DMS-1115705. The last author is grateful for funding provided by the AFOSR under grant number FA9550-12-1-0115.

REFERENCES

[1] Friedlander, S. K., 2000. *Smoke, dust, and haze*, vol. 198. Oxford University Press New York.

[2] Gidaspow, D., 1994. *Multiphase flow and fluidization: continuum and kinetic theory descriptions*. Academic Press.

[3] Kieffer, S. W., and Sturtevant, B., 1984. "Laboratory studies of volcanic jets". Journal of Geophysical Research, **89** (B10) , pp. 8253–8268.

[4] Crowe, C. T., Sharma, M. P., and Stock, D. E., 1977. "The particle-source in cell (psi-cell) model for gas-droplet flows". *J. Fluid Eng.,* **6** , pp. 325–332.

[5] Jacobs, G. B., and Don, W. S., 2009. "A high-order weno-z finite difference based particle-source-in-cell method for computation of particle-laden flows with shocks". *J. Comp. Phys.,* **5** , p. 228.

[6] Sengupta, K., Shotorban, B., Jacobs, G. B., and Mashayek, F., 2009. "Spectral-based simulations of particle-laden turbulent flows". *Int. J. of Multiphase Flow,* **35** , p. 811.

[7] Balachandar, S., 2009. "A scaling analysis for point-particle approaches to turbulent multiphase flows". *Int. J. of Multiphase Flow,* **35** , p. 801.

[8] Balachandar, S., and Eaton, J. K., 2010. "Turbulent dispersed multiphase flow". *Annual Review of Fluid Mechanics,* **42** , p. 111.

[9] Anderson, T. B., and Jackson, R., 1967. "A fluid mechanical description of fluidized beds". *Ind. Eng Chem. Fundam.,* **6** , p. 527.
[10] Jackson, R., 1997. "Locally averaged equations of motion for a mixture of identical spherical particles and a newtonian fluid". *Chem. Eng. Sci.,* **52** , p. 2457.
[11] Joseph, D. D., Lundgren, T. S., Jackson, R., and Saville, D. A., 1990. "Ensemble averaged and mixture theory equations for incompressible particle suspension". *Int. J. Multiphase Flow,* **16** , p. 35.
[12] Zhang, D. Z., and Prosperetii, A., 1997. "Momentum and energy equation for disperse two-phase flows and their closure for dilute suspensions". *Int. J. Multiphase Flow,* **23** , p. 425.
[13] Pandya, R. V. R., and Mashayek, F., 2002. "Two-fluid large-eddy simulation approach for particle-laden turbulent flows". *Int. J. Heat Mass Transfer,* **6** , p. 4753.
[14] Fox, R. O., 2012. "Large-eddy-simulation tools for multiphase flows". Annual Review of Fluid Mechanics, **44** (1) , pp. 47–76.
[15] Shotorban, B., 2011. "Preliminary assesment of two-fluid model for direct numerical simulation of particle-laden flows". *AIAA Journal,* **49** , pp. 438–443.
[16] Ortiz, O., 2011. Eulerian-Eulerian model of 1-D compressible particle-laden flow: Running shock impinging on a cloud of particle. Master's thesis, San Diego State University, San Diego, CA.
[17] Truong, Q. T., 2012. Eulerian-Eulerian model for computation of a 2-D compressible particle-laden flow. Master's thesis, San Diego State University, San Diego, CA.
[18] LeVeque, R. J., 2002. *Finite Volume Methods for Hyperbolic Problems*. Cambridge University Press, New York, NY.

Table 1: Initial Conditions of the Domain in the 2-D Case

x_1	x_2	y_1	y_2	x_{p1}	x_{p2}	y_{p1}	y_{p2}
0	1	-0.2	0.2	0	0.2981	0.175	0.352

Table 2: Initial Conditions of the Carrier Phase in the 2-D Case

M_s	γ	Pr	β	St	p	ρ	u_1	u_2
3.0	1.4	1.67	0.4	1	1	1	0	0

Table 3: Initial Conditions of the Particle Phase in the 2-D Case

N_p	d_p	ρ_p	ϕ
40000	5.7693E-3	1000	2.2599E6

v_1	v_2	θ	σ_{11}	σ_{12}	σ_{22}	q_1	q_2
0	0	T_f	0	0	0	0	0

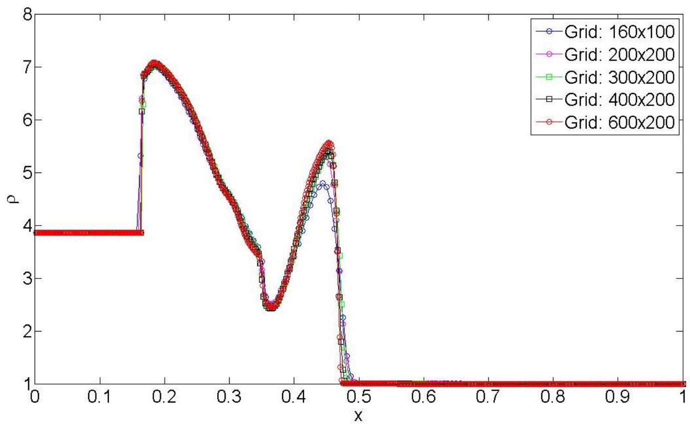

Figure 1: Carrier phase density ρ versus x on the symmetry line $y = 0$, at $t = 0.1$ of the EE model at different grid size. Parameters used in the simulation are given in Tables 2 and 3.

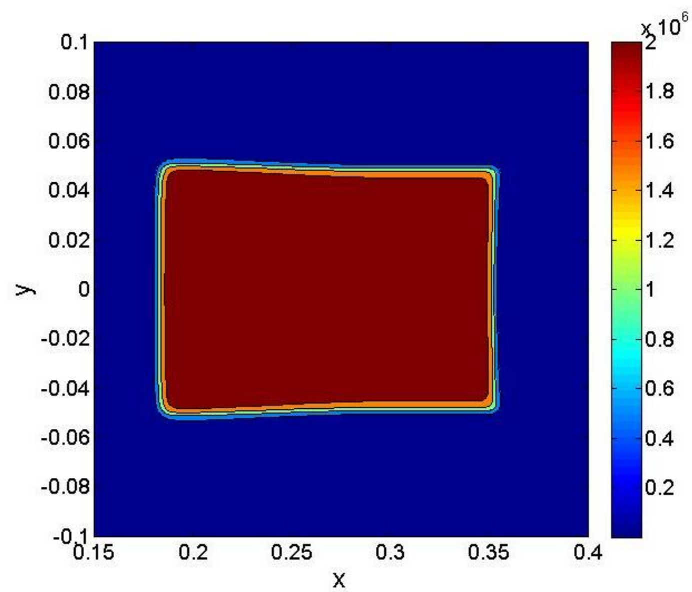

Figure 2: Contour plot of the particle number density ϕ at $t = 0.1$ of the EE model. Parameters used in the simulation are given in Tables 2 and 3.

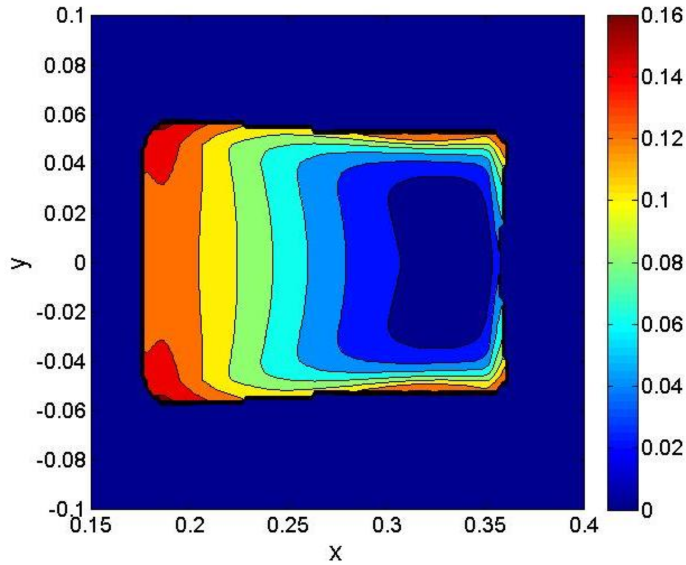

Figure 3: Contour plot the particle x-component velocity v_1 at $t = 0.1$ of the EE model. Parameters used in the simulation are given in Tables 2 and 3.

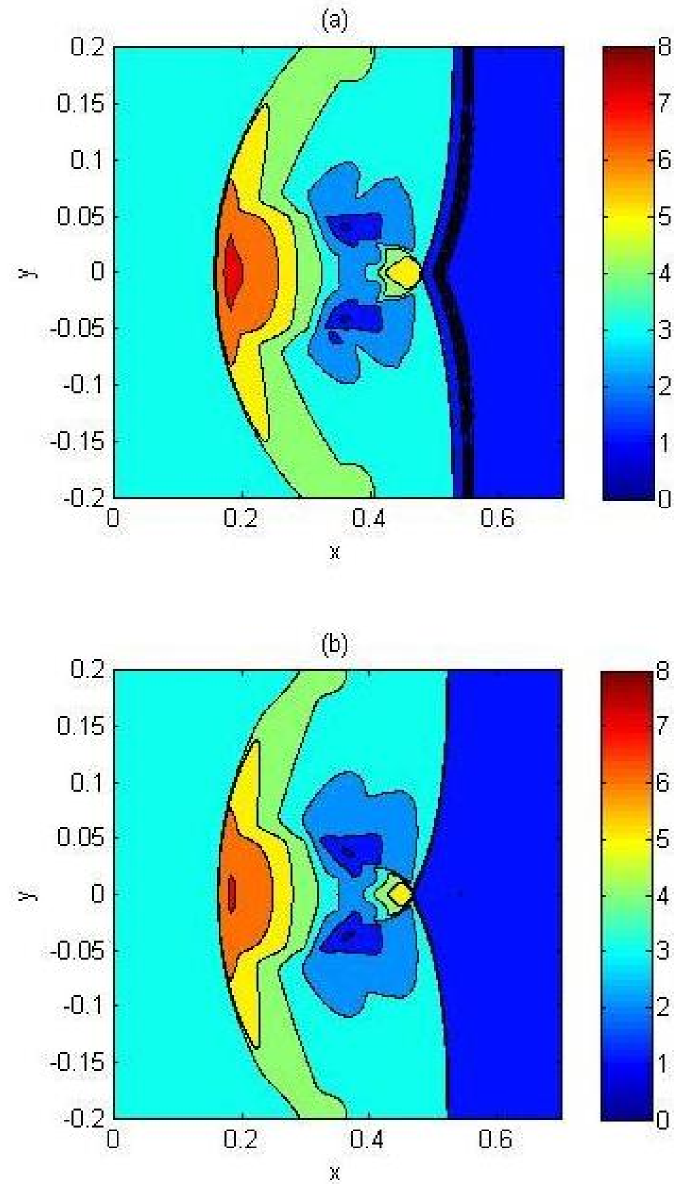

Figure 4: Contour plot of fluid density ρ at $t = 0.1$ computed by (a) EL model (WENO-5); and (b) EE model.

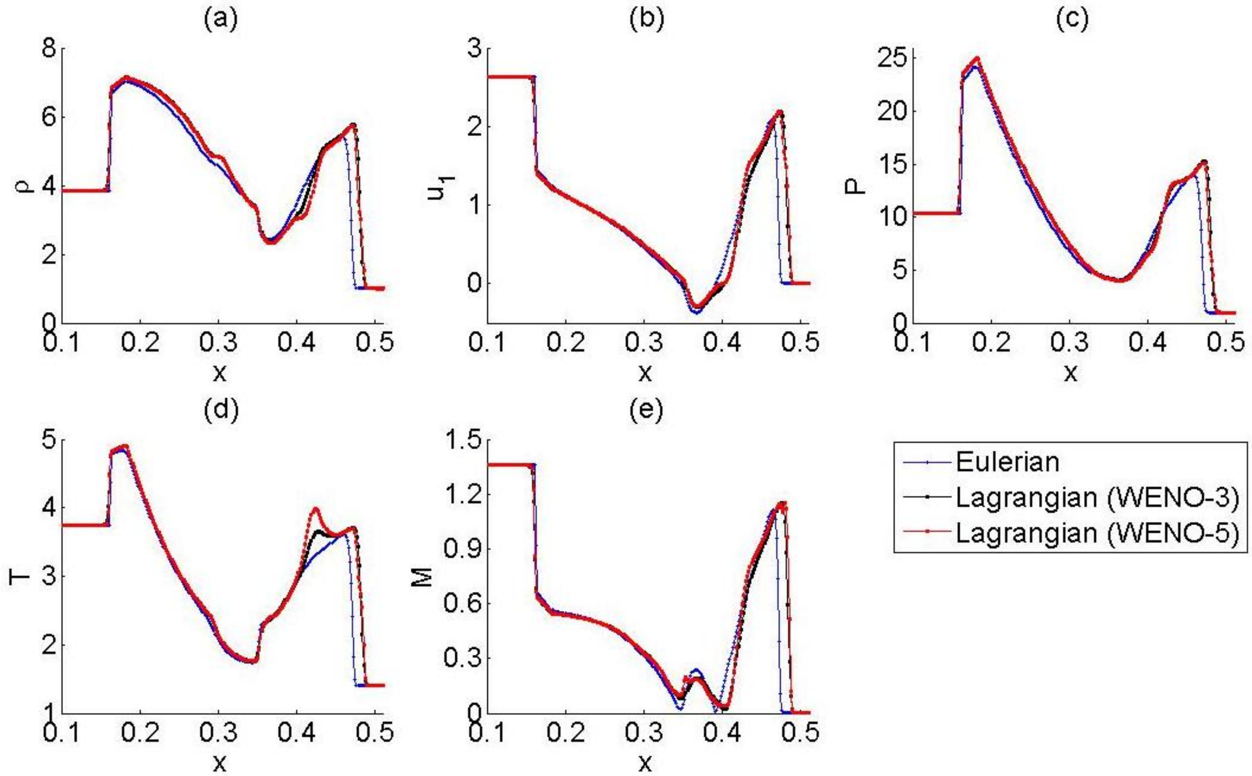

Figure 5: Fluid properties versus x on the symmetry line $y = 0$ at $t = 0.1$: (a) density; (b) velocity component at x direction; (c) pressure; (d) temperature; and (e) Mach number.

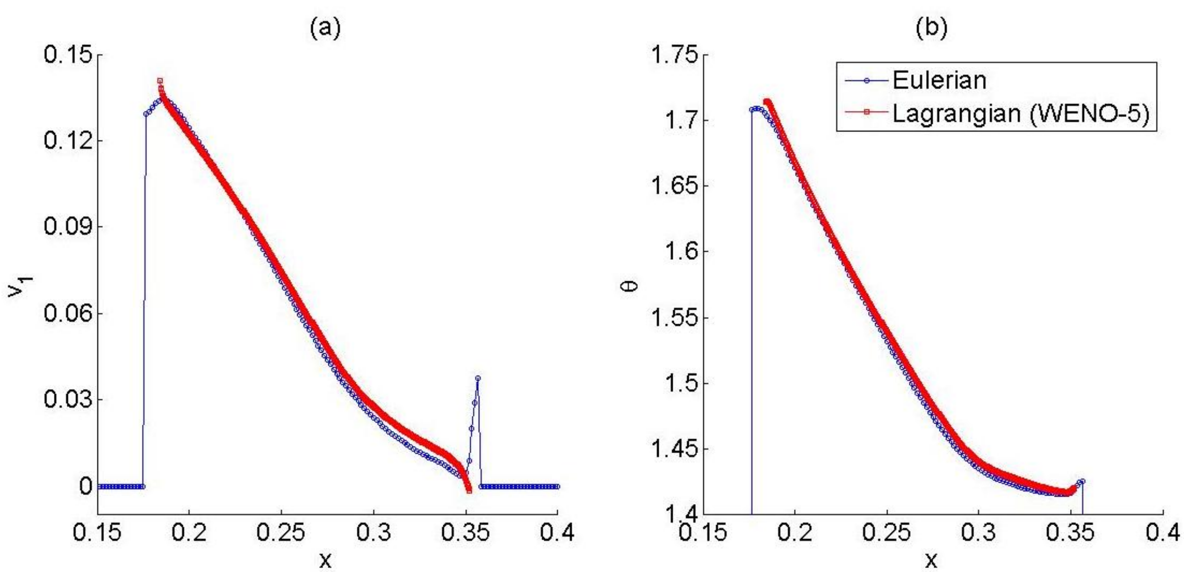

Figure 6: Fluid properties versus x on the symmetry line $y = 0$ at $t = 0.1$: (a) particle velocity; (b) particle temperature.